CrossMark

ORIGINAL PAPER

Adaptive reactionless control strategy via the PSO-ELM algorithm for free-floating space robots during manipulation of unknown objects

Zhongyi Chu · Ye Ma · Jing Cui

Abstract The operation of free-floating space robots causes significant challenges to the attitude control of a spacecraft body, resulting from the strong dynamic coupling existing in the system as well as the appending unknown property from a captured object. Conventional reactionless motion planning and control methods require the precise knowledge of system dynamics with ideal path tracking performance, which are impossible to achieve in reality. To solve this problem, an adaptive reactionless path planning and control integrated strategy is proposed for free-floating space robots while manipulating unknown objects. For details, a SW-RLS (Slide-windowed Recursive Least Square) algorithm is employed to construct the adaptive reactionless path planning by identifying and compensating the unknown property in the form of a time-variable matrix for the momentum equation of the system. Simultaneously, a robust adaptive control strategy via the PSO-ELM (Particle Swarm Optimization-Extreme Learning Machine) algorithm is proposed to track the dynamic change in the planned path, based on the foundation of a designed PD controller for reducing the error. With computational efficiency, an adaptive controller via PSO-ELM aims at learning and compensating for the unknown property intelligently; then, a robust controller is used to reject the model uncertainties. The notable feature of the proposed strategy is that it requires neither an accurate system model nor any information about the unknown property. Most importantly, the design can dynamically realize reactionless path tracking performance. Finally, the simulations of a free-floating space robot capturing an unknown object and comparisons with existing methods are presented to demonstrate the effectiveness of the proposed scheme.

Z. Chu · Y. Ma
School of Instrument Science and Opto-electronics,
Beihang University, Beijing 100191, China

J. Cui (✉)
School of Mechanical Engineering and Application
Electronic, Beijing University of Technology, Beijing
100191, China
e-mail: cuijing@bjut.edu.cn

Nomenclature

M	Dynamic inertial matrix
C	Matrix that incorporates centrifugal force and Coriolis force
d	Interior disturbance vector
τ	Generalized force vector
q	Generalized variable
D	Composite disturbance vector
a_i	Position vector from joint i to centroid of link i
b_i	Position vector from center of link i to joint $(i+1)$

Springer

b_B	Position vector from center of spacecraft body to joint 1
r_i	Position vector of link i with respect to inertial frame
r_g	Position vector of the whole system with respect to inertial frame
m	Total mass of robotic system
m_i	Mass of link i
I_i	Inertial tensor of z axis of joint i
n	Amount of joints
r	System error of control
e	Position tracking error
Λ	Diagonal matrix with positive diagonal elements
P	Linear momentum of the whole system
L	Angular momentum of the whole system
v_0	Linear velocity of spacecraft body
ω_0	Angular velocity of spacecraft body
α	Attitude angle of spacecraft body
θ_i	Angle of joint i
I	Identity matrix
ε_1	Priori residual error
ε_2	Posteriori residual error
PN	Inverse of autocorrelation matrix
x_i	Input vector of ith ELM network
A_i	Input weight matrix of ith ELM network
b_i	Hidden bias of ith ELM network
g_i	Activation function of ith ELM network
β_i	Output weight matrix of ith ELM network
l	Amount of hidden layer nodes of ELM network
γ	Step-length regulatory factor of ELM network
m	Amount of optimized particles
S	Set of optimized particles
p_i	Best partial position for particle i
g_i	Best global position for particle i
K	Positive definite matrix

1 Introduction

The utilization of space robots [1] is of paramount importance with the increase in space operations including assembly, capturing and construction. Various special tasks (e.g., removal of space debris) can pose a threat to the robotic systems because of the unknown properties of captured objects. In fact, capturing operations by a space robot installed on the spacecraft body need to be limited when the entire system works in a free-floating state [2]. A strong dynamic coupling relationship exists between the spacecraft body and the robotic arm, and the motion of the space robot will lead to instability of the spacecraft body attitude. The ACS (Attitude Control System) of the spacecraft can be employed to ensure the stability of the entire system but with large fuel consumption. The proper path planning of the robotic arm can counteract this effect on the motion of the space robot on spacecraft attitude. No energy problem exists because the sustainable electric energy produced by a solar array can be employed [3]. However, the uncertain properties from the captured unknown object such as space debris can cause the conventional no-disturbance planning methods to be invalid; therefore, precise dynamic knowledge of the entire system is required by the RNS (Reaction Null Space) algorithm or similar [4–7]. An "identification" process during the post-capture stage was introduced [8–11] by measuring the property of the captured object and compensating for the path planning and control system. Similar schemes should acquire accurate information of the captured object and bring about high sensor requirements and a delay control issue. To solve this problem, the ARNS (Adaptive Reaction Null Space) method with dynamic changing planning paths for robotic arms [3] during capturing of an unknown object was proposed and introduced to realize the minimum disturbance to the spacecraft body attitude. In this method, the unknown part of the system (the captured object) can be obtained online via the RLS (Recursive Least Square) algorithm and compensation can be made in the form of a time-variable matrix for the path planning equation of the robotic arm. Thus, the delay control issue is solved. The conventional RLS algorithm employed in ARNS exhibits saturation characteristics [12] with the growth of the gain matrix caused by the increased computation, and the online identification for the time-variable term that incorporates the unknown property to construct the planned path will expire, thereby degrading the performance of the path via ARNS. RLS via the forgetting factor [13] could make the ARNS improve its adaptability with limited ability. Furthermore, the SW-RLS algorithm [14]

focuses more on the rapidly changed parameters of time-varying systems, and there is no saturation characteristic based on retaining the limited data length by eliminating the older history data.

To realize the reactionless motion for a space robot while capturing an unknown object, an effective reactionless path planning with dynamical changing features is essential. Simultaneously, an efficient control strategy to track the planned path of the space robot is well worth considering because the scheme to realize reactionless motion such as ARNS usually involves ideal path tracking performance, which neglects the effect of the tracking error from the controller and is impossible in reality. To degrade the effects of tracking errors, the control strategy for the controller requires faster tracking speed and less tracking errors to ensure better attitude stability performance for the entire system. Considering the complicated disturbance existing in the control system, such as the abrupt and uncertain changes in system dynamics by capturing an unknown object as well as the original modeling uncertainty of the system, the control strategy to track the adaptive path of a robotic arm needs to be robust and adaptive. Therefore, a single robust controller [15–17] or an adaptive controller [18–20] can hardly ensure the control performance in capturing the unknown object with abrupt uncertain properties. A compromise is developed with the robust adaptive control strategy [21–24] to adopt the advantages from both the control strategy, by which the unknown disturbance is learned and compensated via the adaptive strategy, and to reject the model uncertainties via the robust strategy. However, different from the conventional strategy of using the adaptive control to learn the unknown parts of the dynamic system, the space-capturing task attached with the abrupt change in dynamics needs a faster learning and compensating method for the abrupt unknown properties. Traditional adaptive control methods such as a BP (Back Propagation) network [25], RBF (Radial Basis Function) network [25] and fuzzy algorithm [21,22] exhibit complicated computing processes and are insufficient to deal with the abrupt properties or ensure adaptive speed. Recently, the ELM [26] algorithm was developed for its extremely fast system uncertainty learning and cognizing performance [27,28]. However, the random input feature settings (input weight, hidden layer bias) of conventional ELM networks could weaken the network performance to

some extent because the pre-setting input feature owns the possibility of staying away from its optimal value.

Given the problem, some ameliorated methods by optimizing the input feature of the ELM algorithm have been proposed. Zhu et al. [29] used various types of evolutionary algorithms to determine network input features, which achieved better generalization performance with more compact networks. Particle Swarm Optimization (PSO) was combined with the ELM algorithm in [30] to improve the generalization capacity of the SLFNs (Single-hidden Layer Feed-forward Networks). Xu et al. [31] proposed an evolutionary ELM based on PSO, which can address certain prediction problems more suitably. Han et al. presented an improved ELM algorithm with improved PSO via adaptive inertia in [32] to choose the input feature of the SLFN. In addition, a performance investigation through the PSO-ELM algorithm with various alternative topologies is presented in [33]. The research above with the optimization of the input features of ELM via the PSO algorithm exhibits strong advantages including online parameter adjustment, avoiding optimal input feature value and enhancing the ELM performance. Therefore, in order to satisfy the requirements of faster adaptive performance and higher tracking accuracy for space robots to track the reactionless path, considering the abrupt unknown properties of the manipulating task, a dynamical identification and control strategy without saturation characteristics is developed. This strategy addresses the time-variable matrix for constructing the reactionless path and is necessary to achieve an improved ELM algorithm.

In this paper, an adaptive reactionless path planning and control integrated strategy is proposed for a free-floating space robot while capturing an unknown object, and the work is presented as follows:

(1) An adaptive reactionless path planning method is proposed for a space robot, which employs the SW-RLS algorithm to identify and compensate for the unknown properties existing in the system and simultaneously avoids the saturation phenomenon when dealing with time-variable elements during planning.
(2) A robust adaptive control strategy is proposed for space robots to track the planned reactionless path, which employs the PSO-ELM algorithm to dynamically learn and compensate for the unknown properties in the form of constructed

adaptive control. Herein, the ELM algorithm is used to address the abrupt properties according to its extremely fast learning performance, and the PSO algorithm is used to optimize the input feature of ELM to avoid the optimal value and also to enhance ELM performance. In addition, the designed PD controller is employed to reduce errors associated with computational efficiency, and the robust controller is applied to reject the model uncertainties.

(3) To verify the validity of the proposed strategy, simulations of a free-floating space robot with a 4-DOF (Degree of Freedom) robotic arm capturing an unknown object and comparisons with other existing methods are implemented and presented.

This paper is organized as follows. Part II presents the basic dynamic relationship for a free-floating space robot in the post-capture stage, and a dynamic decoupling derivation for the robotic arm is described to construct the basis of the joint controller design. Part III illustrates the form of the ARNS algorithm via SW-RLS algorithm to plan the adaptive reactionless path for the robotic arm, and the details of the proposed robust adaptive control strategy via PSO-ELM are discussed to track the planned path. In Part IV, the simulation is conducted by comparing the performance of the proposed strategy with other conventional strategies. Part V presents the conclusion.

2 Basic dynamics of a free-floating space robot

Figure 1 shows a schematic diagram and the vital parameters of a space robot composed of a rigid serial-link robotic arm and the spacecraft. The vectors r_b, r_i and r_g denote the centroid position of the spacecraft, link i and the entire robotic system, respectively, expressed in inertial frame. Considering that the system works in a free-floating state without any external forces or torque, i.e., without the employment of momentum exchange devices, the only disturbances of the robotic system are derived from interior factors such as joint friction, measurement noises and model uncertainty. Thus, the robotic system is subject to the law of linear and angular momentum conservation in the post-capture stage. The detailed kinematics and dynamics of a space robot can be found in [2], by which the dynamic equation can be rewritten as follows.
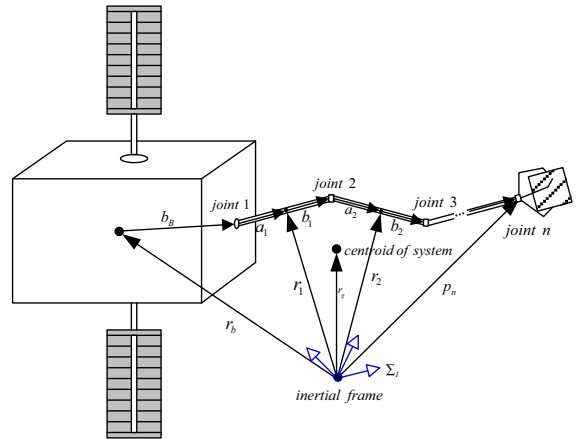

Fig. 1 Space robot in the post-capture stage

From [2], the basic dynamic equation of the system before capturing can be expressed by Eq. (1).

$$M(q)\ddot{q} + C(q,\dot{q})\dot{q} + d = \tau \tag{1}$$

Equation (1) illustrates the precise dynamic knowledge of the whole system in the pre-capture stage, without the property of captured object, and the dynamic parameters are regarded as prior data. The matrix $M(q)$ in Eq. (1) denotes the dynamic inertial matrix of the system, and $C(q,\dot{q})$ contains the centrifugal force and Coriolis force of the system; d denotes the interior disturbance term, and τ is the generalized force composed of the actuating torque of the motors installed on each joint; q denotes the generalized variable term, which is composed of the angular displacement of each joint.

Given the capturing operation involving an unknown object with appending dynamic parameters, the dynamic parameters of the entire system might be changed, and the dynamic equation of the entire system in the post-capture stage will be rewritten again as Eq. (2). In this equation, $\hat{M}(q)$ and $\hat{C}(q,\dot{q})$ contain the uncertain properties from the captured object, so the uncertain dynamic parameter can be defined by Eq. (3),

$$\hat{M}(q)\ddot{q} + \hat{C}(q,\dot{q})\dot{q} + d = \tau$$
$$\tilde{M}(q) = \hat{M}(q) - M(q) \tag{2}$$
$$\tilde{C}(q,\dot{q}) = \hat{C}(q,\dot{q}) - C(q,\dot{q}) \tag{3}$$

where $\tilde{M}(q)$ and $\tilde{C}(q,\dot{q})$ result from the captured object.

To simplify the form of the existing uncertainties in the system, the composite disturbance D is defined with

Eq. (4) that includes the unknown properties as well as the interior disturbance d.

$$\tau = \hat{M}(q)\ddot{q} + \hat{C}(q,\dot{q})\dot{q} + d$$
$$= M(q)\ddot{q} + C(q,\dot{q})\dot{q} + d + \tilde{M}(q)\ddot{q} + \tilde{C}(q,\dot{q})\dot{q}$$
$$= M(q)\ddot{q} + C(q,\dot{q})\dot{q} + D$$
$$D = d + \tilde{M}(q)\ddot{q} + \tilde{C}(q,\dot{q})\dot{q} \tag{4}$$

$M(q) = diag\{M_{11} \ldots M_{ii} \ldots M_{nn}\}$ in Eq.(4) is a constant diagonal matrix with n×n elements, i.e., M_{ii} is a constant-valued nominal term of the ith subsystem via axis inertia. Therefore, Eq. (4) can be rewritten by Eq. (5).

$$\ddot{q} = -M(q)^{-1}(C(q,\dot{q})\dot{q} + D) + M(q)^{-1}\tau \tag{5}$$

Now, combining the term $-M(q)^{-1}(C(q,\dot{q})\dot{q}+D)$ into a newly defined uncertain term D', the dynamic Eq. (5) can be transformed into Eq. (6),

$$\ddot{q} = D' + M(q)^{-1}\tau \tag{6}$$

where $D' = (D'(1)\ D'(2) \ldots D'(n))$.

Noting that $M(q)$ is invertible with a diagonal form, it is straightforward to verify that Eq. (6) can be decoupled through the proper transformation. The decoupled form is illustrated by Eq. (7), with an uncertain $D'(i)$ for the ith subsystem.

$$\ddot{q}_i = D'(i) + M_{ii}^{-1}\tau_i \tag{7}$$

Then, the system error of control r for the robotic system is redefined and expressed as Eq. (8),

$$r = \dot{e} + \Lambda e$$
$$\dot{e} = \dot{q} - \dot{q}_d$$
$$e = q - q_d \tag{8}$$

where q and q_d denote the actual and desired generalized variable terms, respectively, and $\dot{q}$ and $\dot{q}_d$ denote the derivation of them, respectively. e represents the position tracking error, and Λ represents the diagonal matrix with positive diagonal elements. Therefore, the reference output $\dot{q}_r$ can be defined and expressed via Eq. (9a) and fulfill the relationship via Eq. (9b) based on Eqs. (4) and (8).

$$\dot{q}_r = \dot{q}_d + \Lambda e \tag{9a}$$
$$M\ddot{q}_r + C\dot{q}_r + D - \tau = M(\ddot{q}_d + \Lambda\dot{e})$$
$$\quad + C(\dot{q}_d + \Lambda e) + D - (M\ddot{q} + C\dot{q} + D)$$
$$= M(\ddot{q}_d + \Lambda\dot{e} - \ddot{q}) + C(\dot{q}_d + \Lambda e - \dot{q})$$
$$= M(\ddot{e} + \Lambda\dot{e}) + C(\dot{e} + \Lambda e)$$
$$= M\dot{r} + Cr \tag{9b}$$

3 Adaptive reactionless control strategy

To realize the reactionless motion of the robotic arm, the integrated adaptive reactionless control strategy involves adaptive path planning and the corresponding control strategy. The adaptive path planning would be adaptively updated by the SW-RLS because of the existing time-variable elements in the coefficient matrix of the ARNS algorithm. In addition, the robust adaptive control strategy via PSO-ELM algorithm is proposed to fast track the planned adaptive path of the robotic arm to ensure enough robustness and the adaptive nature of the system control performance. The schematic of the proposed adaptive reactionless control strategy is illustrated in Fig. 2.

3.1 Adaptive reactionless path planning via SW-RLS

The space robot is subject to the law of linear/angular momentum conservation when the system operates in

Fig. 2 Adaptive reactionless control strategy for space robotic

Robust Adaptive Control Strategy

Reactionless Path

Joint Controller Design

Space Robotic Arm

Time-variable Element Update

SW - RLS algorithm

Adaptive Reactionless Path Planning
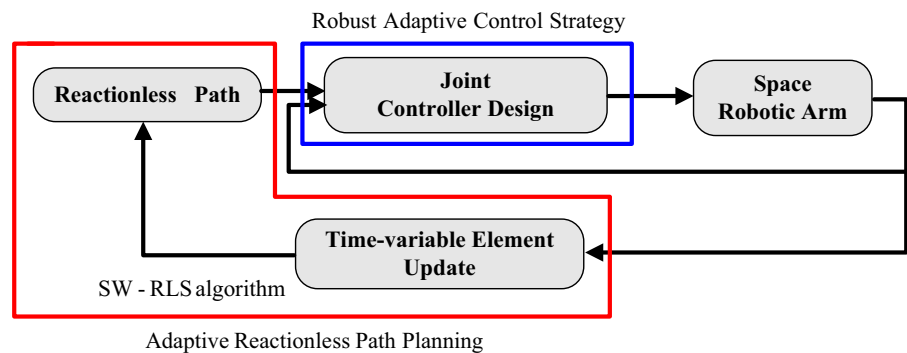
the post-capture stage, and thereby, the total linear and angular momentum of the system can be reformed by Eq. (10) according to [3], with expressed $\boldsymbol{P}$ (linear momentum) and $\boldsymbol{L}$ (angular momentum), respectively.

$$\begin{bmatrix} \boldsymbol{P} \\ \boldsymbol{L} \end{bmatrix} = \begin{bmatrix} m\boldsymbol{I} & m\tilde{\boldsymbol{r}}_{0g}^T \\ 0 & \boldsymbol{H}_\omega \end{bmatrix} \begin{bmatrix} \boldsymbol{v}_0 \\ \boldsymbol{\omega}_0 \end{bmatrix} + \begin{bmatrix} \boldsymbol{J}_{T\omega} \\ \boldsymbol{H}_{\omega\phi} \end{bmatrix} \dot{\boldsymbol{q}} + \begin{bmatrix} 0 \\ \boldsymbol{r}_g \times \boldsymbol{P} \end{bmatrix} \tag{10}$$

In the above, the expressions $\boldsymbol{v}_0$ and $\boldsymbol{\omega}_0$ represent the linear velocity and angular velocity of the spacecraft, respectively, expressed in the inertial frame; $\dot{\boldsymbol{q}}$ represents the derivation of the generalized variable $\boldsymbol{q}$, i.e., joint rate; m denotes the total mass of the robotic system; and $\boldsymbol{I}$ is the identity matrix. The coefficient matrix of $[\boldsymbol{v}_0 \ \boldsymbol{\omega}_0]^{\mathrm{T}}$ and $\dot{\boldsymbol{q}}$ is based on the inertial matrix and coupling inertial matrix, accordingly.

Given the angular momentum of the robotic system from Eq. (10), with initial momentum $\boldsymbol{P}_0$, $\boldsymbol{L}_0$ is expressed as follows:

$$\boldsymbol{L} = \boldsymbol{H}_\omega \boldsymbol{\omega}_0 + \boldsymbol{H}_{\omega\phi} \dot{\boldsymbol{q}} + \boldsymbol{r}_g \times \boldsymbol{P}_0 = \boldsymbol{L}_0 \tag{11}$$

i.e.,

$$\boldsymbol{H}_\omega \boldsymbol{\omega}_0 + \boldsymbol{H}_{\omega\phi} \dot{\boldsymbol{q}} = \boldsymbol{L}_0 - \boldsymbol{r}_g \times \boldsymbol{P}_0 \tag{12}$$

Based on the RNS algorithm [4–7], the desired path planning of the robotic arm to realize reactionless motion for the spacecraft can be obtained by Eq. (13),

$$\dot{\boldsymbol{q}}_{d|\mathrm{RNS}} = \boldsymbol{H}_{\omega\phi}^+ (\boldsymbol{L}_0 - \boldsymbol{r}_g \times \boldsymbol{P}_0) + (\boldsymbol{I} - \boldsymbol{H}_{\omega\phi}^+ \boldsymbol{H}_{\omega\phi}) \dot{\boldsymbol{\zeta}} \tag{13}$$

where $\dot{\boldsymbol{\zeta}}$ is the arbitrary vector ($\dot{\boldsymbol{\zeta}} \in \boldsymbol{R}^n$) mapped into the null space of $\boldsymbol{H}_{\omega\phi}$, and to ensure the initial velocity of each joint is available, the $\dot{\boldsymbol{\zeta}}$ should be defined as a vector with nonzero elements [3–7]; $\boldsymbol{H}_{\omega\phi}^+$ represents the pseudo-inverse of $\boldsymbol{H}_{\omega\phi}$.

Then, considering the captured unknown object with unknown properties, the coefficient matrix (base inertial matrix, coupling inertial matrix) incorporating the uncertain dynamic parameter cannot be obtained precisely, which affects the desired path $\dot{\boldsymbol{q}}_{\mathrm{RNS}}$ to realize the absolutely reactionless motion. Therefore, the ARNS algorithm is employed to realize the adjustment online for the coefficient matrix to obtain the precise property of the post-capture system.

Equation (12) is rewritten, illustrated by Eq. (14), in which the signal $\wedge$ represents the current estimate value that incorporates the dynamic parameter of the captured unknown object. Then, Eqs. (13) and (14) are combined and expressed by Eq. (15),

$$\dot{\boldsymbol{q}} = \hat{\boldsymbol{H}}_{\omega\phi}^+ (\boldsymbol{L}_0 - \boldsymbol{r}_g \times \boldsymbol{P}_0) - \hat{\boldsymbol{H}}_{\omega\phi}^+ \hat{\boldsymbol{H}}_\omega \boldsymbol{\omega}_0$$
$$+ \left(\boldsymbol{I} - \hat{\boldsymbol{H}}_{\omega\phi}^+ \hat{\boldsymbol{H}}_{\omega\phi} \right) \dot{\boldsymbol{\zeta}} \tag{14}$$

$$\dot{\boldsymbol{q}}_{d|\mathrm{RNS}} - \dot{\boldsymbol{q}} = (\boldsymbol{H}_{\omega\phi}^+ - \hat{\boldsymbol{H}}_{\omega\phi}^+)(\boldsymbol{L}_0 - \boldsymbol{r}_g \times \boldsymbol{P}_0)$$
$$+ \hat{\boldsymbol{H}}_{\omega\phi}^+ \hat{\boldsymbol{H}}_\omega \boldsymbol{\omega}_0 + (\hat{\boldsymbol{H}}_{\omega\phi}^+ \hat{\boldsymbol{H}}_{\omega\phi} - \boldsymbol{H}_{\omega\phi}^+ \boldsymbol{H}_{\omega\phi}) \dot{\boldsymbol{\zeta}}$$
$$= [\boldsymbol{K}_1 \boldsymbol{K}_2 \boldsymbol{K}_3] \begin{bmatrix} \boldsymbol{1} \\ \boldsymbol{\omega}_0 \\ \dot{\boldsymbol{\zeta}} \end{bmatrix} \tag{15}$$

where matrix $\boldsymbol{K}_1$, $\boldsymbol{K}_2$ and $\boldsymbol{K}_3$ owns the time-variable elements, expressed as follows.

$$\boldsymbol{K}_1 = \left(\boldsymbol{H}_{\omega\phi}^+ - \hat{\boldsymbol{H}}_{\omega\phi}^+ \right) (\boldsymbol{L}_0 - \boldsymbol{r}_g \times \boldsymbol{P}_0)$$
$$\boldsymbol{K}_2 = \hat{\boldsymbol{H}}_{\omega\phi}^+ \hat{\boldsymbol{H}}_\omega$$
$$\boldsymbol{K}_3 = \left(\hat{\boldsymbol{H}}_{\omega\phi}^+ \hat{\boldsymbol{H}}_{\omega\phi} - \boldsymbol{H}_{\omega\phi}^+ \boldsymbol{H}_{\omega\phi} \right) \tag{16}$$

Based on Eq. (15), the precise coefficient matrix $\boldsymbol{K}_1$, $\boldsymbol{K}_2$ and $\boldsymbol{K}_3$ means that $\dot{\boldsymbol{q}}$ can ultimately converge to the desired path $\dot{\boldsymbol{q}}_{d|\mathrm{RNS}}$ to realize reactionless motion for the robotic arm [3]. Thus, the identification algorithm SW-RLS is used to obtain the coefficient matrix online to deal with the time-variable parameters from $\boldsymbol{K}_1$, $\boldsymbol{K}_2$ and $\boldsymbol{K}_3$. The simplified linear regression forms of Eq. (15) are defined with Eq. (17) as follows:

$$\boldsymbol{\Psi}\boldsymbol{\Theta} = \boldsymbol{\Phi} \tag{17}$$

where $\boldsymbol{\Theta}$ denotes the coefficient matrix $[\boldsymbol{K}_1 \boldsymbol{K}_2 \boldsymbol{K}_3]^T$; $\boldsymbol{\Psi}$, $\boldsymbol{\Phi}$ denote the terms $\begin{bmatrix} 1 \ \boldsymbol{\omega}_0 \ \dot{\boldsymbol{\zeta}} \end{bmatrix}^{\mathrm{T}}$ and $[\dot{\boldsymbol{q}}_{d|\mathrm{RNS}} - \dot{\boldsymbol{q}}]^{\mathrm{T}}$, respectively.

The details of the SW-RLS algorithm can be found in [14] and are expressed below with Eq. (18). New data are being added to the algorithm via Eq. (18a), and the older data are removed via Eq. (18b) to avoid the saturation phenomenon. From Eq. (18), k denotes the kth iteration for the corresponding elements and $\hat{\boldsymbol{\Theta}}_{(k)}$ is an estimate of $\boldsymbol{\Theta}$ from iteration k; u denotes the length of the slide window; $\boldsymbol{\varepsilon}_1$ and $\boldsymbol{\varepsilon}_2$ denote the priori and posteriori residual error, respectively; $\boldsymbol{PN}$ is the inverse of the autocorrelation matrix with the initial setting $\boldsymbol{PN}_{(0)} = \delta\boldsymbol{I}$ for $\delta > 1$.

Fig. 3 Proposed control strategy for the joint controller
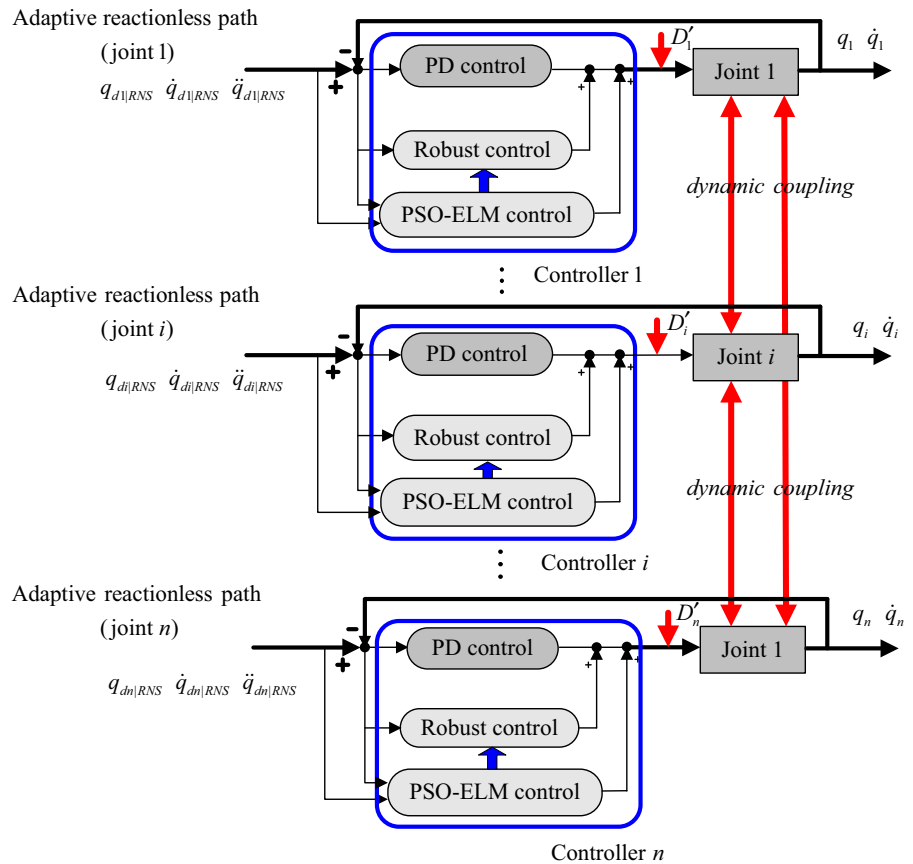
$$\boldsymbol{\varepsilon}_1 = \boldsymbol{\Phi}_{(k+1)} - \boldsymbol{\Psi}_{(k+1)}\hat{\boldsymbol{\Theta}}_{(k)}$$

$$\Delta_{1(k+1)} = \frac{\boldsymbol{PN}_{(k)}\boldsymbol{\Psi}_{(k+1)}}{\boldsymbol{I} + \boldsymbol{\Psi}_{(k+1)}^{\mathrm{T}}\boldsymbol{PN}_{(k)}\boldsymbol{\Psi}_{(k+1)}} \quad (18a)$$

$$\boldsymbol{PN}_{1(k+1)} = [\boldsymbol{I} - \Delta_{1(k+1)}\boldsymbol{\Psi}_{(k+1)}^{\mathrm{T}}]\boldsymbol{PN}_{(k)}$$

$$\hat{\boldsymbol{\Theta}}_{1(k+1)} = \hat{\boldsymbol{\Theta}}_{(k)} + \Delta_{1(k+1)}\boldsymbol{\varepsilon}_1$$

$$\boldsymbol{\varepsilon}_2 = \boldsymbol{\Phi}_{(k-u+1)} - \boldsymbol{\Psi}_{(k-u+1)}\hat{\boldsymbol{\Theta}}_{1(k+1)}$$

$$\Delta_{(k+1)} = \frac{\boldsymbol{PN}_{1(k+1)}\boldsymbol{\Psi}_{(k-u+1)}}{-\boldsymbol{I} + \boldsymbol{\Psi}_{(k-u+1)}^{\mathrm{T}}\boldsymbol{PN}_{1(k+1)}\boldsymbol{\Psi}_{(k-u+1)}}$$

$$\boldsymbol{PN}_{(k+1)} = [\boldsymbol{I} - \Delta_{(k+1)}\boldsymbol{\Psi}_{(k-u+1)}^{\mathrm{T}}]\boldsymbol{PN}_{1(k+1)}$$

$$\hat{\boldsymbol{\Theta}}_{(k+1)} = \hat{\boldsymbol{\Theta}}_{1(k+1)} + \Delta_{(k+1)}\boldsymbol{\varepsilon}_2 \quad (18b)$$

According to the description in Eqs. (15–18), the reactionless path with dynamical changing performance can be obtained, as shown in Eq. (19) as follows:

$$\dot{\boldsymbol{q}}_{d|\mathrm{RNS}} = \dot{\boldsymbol{q}} + \hat{\boldsymbol{\Theta}}\begin{bmatrix} \mathbf{1} \\ \boldsymbol{\omega}_0 \\ \dot{\boldsymbol{\zeta}} \end{bmatrix} \quad (19)$$

in which $\dot{\boldsymbol{q}}_{d|\mathrm{RNS}} = [\dot{q}_{d1|\mathrm{RNS}}, \dot{q}_{d2|\mathrm{RNS}}, \dots, \dot{q}_{dn|\mathrm{RNS}}]^T$ denotes the planned angular velocity for each joint installed on the space robot.

3.2 Robust adaptive control strategy via the PSO-ELM algorithm

In this section, the robust adaptive control strategy using the PSO-ELM algorithm is proposed. According to Eq. (7), in order to compensate for the uncertain term $D'(i)$ for the ith subsystem and to realize the desired tracking for each joint installed on the robotic arm, the proposed control strategy for each joint is preferentially involved through the decoupling Eq. (7) illustrated as Fig. 3.

To address the uncertain term $D'(i)$, the proposed control torque $\bar{\tau}_i$ of joint i takes the form of (20), where τ_{Ai} denotes the adaptive controller to learn and compensate for the uncertain or unknown properties existing in the system. This then employs the ELM algo-
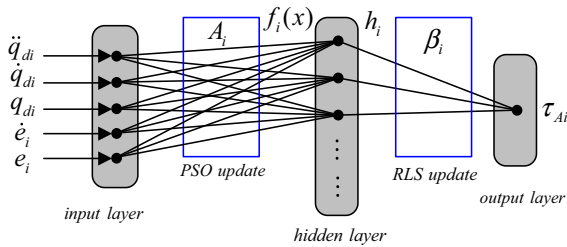
Fig. 4 ELM network diagram

rithm attached with PSO optimization to realize quick tracking and performance enhancement. τ_{Ri} denotes the robust control strategy to reject the model uncertainties, and τ_{PDi} denotes the conventional proportion and differentiation control strategy to reduce the error with computational efficiency.

$$\bar{\tau}_i = M_{ii}(\tau_{Ai} + \tau_{Ri} + \tau_{PDi}) \tag{20}$$

Combining Eqs. (20) and (7) into Eq. (21) is illustrated as follows; thus, the proper choice of τ_{Ai} and τ_{Ri} can compensate for the existing uncertain term $D'(i)$, as described in the next section.

$$D'(i) = \ddot{q}_i - \tau_{Ai} - \tau_{Ri} - \tau_{PDi} \tag{21}$$

3.3 Adaptive control term via the PSO-ELM algorithm

The ELM algorithm is employed to construct an adaptive control strategy to quickly compensate for the abrupt properties of the control system. The PSO algorithm is employed to optimize the input feature of the ELM network to address any input feature variation from the optimal value. The schematic of the PSO-ELM algorithm is illustrated in Fig. 4.

The input vector x_i is defined in Eq. (22) for the network as follows:

$$x_i = [\ddot{q}_{di} \ \dot{q}_{di} \ q_{di} \ e_i \ \dot{e}_i] \tag{22}$$

Therefore, the input and output for the hidden layer can be obtained by Eqs. (23) and (24), respectively, with an input weight matrix A_i, hidden bias b_i and activation function g_i.

$$f_i(x_i) = A_i x_i + b_i \tag{23}$$
$$h_i = g_i(f_i(x_i)) = g_i(A_i x_i + b_i) \tag{24}$$

The output τ_{Ai} of the network can be obtained via Eq. (25), with the output weight matrix $\boldsymbol{\beta}_i$.

$$\tau_{Ai} = h_i \boldsymbol{\beta}_i \tag{25}$$

Therefore, the proposed adaptive law for $\boldsymbol{\beta}_i$ is proposed and presented by Eq. (26) as follows:

$$\dot{\hat{\boldsymbol{\beta}}}_i = [\dot{\hat{\beta}}_{i1} \dot{\hat{\beta}}_{i2} \ldots \dot{\hat{\beta}}_{ij} \ldots]$$
$$\dot{\hat{\beta}}_{ij} = \gamma_{ij} h_i r_i \, (j = 1, 2, \ldots, l)$$
$$\hat{\tau}_{Ai} = h_i \hat{\boldsymbol{\beta}}_i \tag{26}$$

where $\dot{\hat{\boldsymbol{\beta}}}_i$ denotes the estimated growth rate of the estimated weight matrix $\hat{\boldsymbol{\beta}}_i$; l is the amount of hidden layer nodes; γ denotes the step-length regulatory factor; $\hat{\tau}_{Ai}$ represents the estimated output torque, i.e., the output of the adaptive controller. Residual error still exists between $\hat{\tau}_{Ai}$ and τ_{Ai}, compensated by the robust controller exhibited in Sect. 4. The stability analysis of the proposed adaptive law (26) can be verified by the constructed Lyapunov function illustrated below.

To avoid the input weight A_i and the hidden bias b_i of the ELM network varying from the optimal value, A_i and b_i elements are set as the particles requiring optimization, and these elements are reformed into set S, with amount m as follows:

$$S = (s_1, s_2, \ldots, s_i, \ldots, s_m)^T \tag{27}$$

The PSO algorithm is then used to optimize the particles S, according to the principle obtaining the least value of the fitness function $F(S)$, which is chosen by the control tracking error e in this paper. Thus, if the tracking error e exhibits a downtrend, the obtained particles move toward the optimal value. Then, the update via Eq. (28) is adopted; however, if the tracking error is on the rise, the original particle values are maintained.

$$v_i^{k+1} = w v_i^k + c_1 R_1(p_i^k - s_i^k) + c_2 R_2(g_i^k - s_i^k)$$
$$s_i^{k+1} = s_i^k + v_i^{k+1} \tag{28}$$

From Eq. (28), elements s_i and v_i represent the position and velocity of particle i, respectively; p_i and g_i denote the best partial position and best global position for particle i, respectively, obtained by the empirical data from the experimental tests; w denotes the inertial weight serving as a tradeoff between the global and local exploration capabilities of the swarm; c_1 and c_2 are the weights of the stochastic acceleration terms,

determined in advance and pulling each particle toward p_i and g_i; R1 and R2 are the random variables from the range of [0,1]; k denotes the kth iteration for the corresponding elements. To avoid overrun, the limitations for the position and velocity are set as $s_i \in [S_{\min}, S_{\max}]$ and $v_i \in [V_{\min}, V_{\max}]$, respectively.

Therefore, based on Eqs. (27) and (28), particles S, i.e., the optimized input feature A_i, b_i of the ELM network, is associated with improved performance of the adaptive control term via the optimized ELM algorithm.

4 Robust control term

The main purpose for the robust control term in this paper is to reject model uncertainties. The residual errors are produced by the adaptive control process with Eq. (26), i.e., error E_i by Eq. (29), shown as follows:

$$E_i = \tau_{Ai} - \tau_{Ai}^* = h_i \beta_i - h_i \beta_i^* \tag{29}$$

where τ_{Ai}^* denotes the optimal approximation of τ_{Ai}. Noting that there exists an upper bound of E_i with $|E_i| \leq E_{i\_\max}$, the basic form of the robust control term can be illustrated by Eq. (30), where $\hat{\tau}_{Ri}$ represents the estimated output of the robust control term and r_i represents the ith element of system error r.

$$\hat{\tau}_{Ri} = E_{i\_\max} sign(r_i) \tag{30}$$

Therefore, the estimated output of the proposed control strategy $\hat{\tau}$ for the robotic arm can be obtained by Eq. (31) through Eqs. (20) and (30) in which the positive definite matrix K represents the gain of the PD control strategy.

$$\hat{\tau} = [\hat{\tau}_1 \hat{\tau}_2 \dots \hat{\tau}_i \dots \hat{\tau}_n]$$
$$\hat{\tau}_i = \hat{\tau}_{PDi} + \hat{\tau}_{Ai} + \hat{\tau}_{Ri}$$
$$= Kr_i + h_i \hat{\beta}_i + E_{i\_\max} \cdot sign(r_i) \tag{31}$$

5 Stability analysis of the proposed control strategy

Considering the following Lyapunov function:

$$Q = \frac{1}{2} r^T M r + \frac{1}{2} \sum_{i=1}^{n} \sum_{j=1}^{l} \frac{1}{\gamma_{ij}} \tilde{\beta}_{ij} \tilde{\beta}_{ij}$$
$$\tilde{\beta}_{ij} = \hat{\beta}_{ij} - \beta_{ij}^* \tag{32}$$

the first derivation of (32) is derived through Eqs. (9) and (31).

$$\dot{Q} = r^T M \dot{r} + \frac{1}{2} r^T \dot{M} r + \sum_{i=1}^{n} \sum_{j=1}^{l} \frac{1}{\gamma_{ij}} \tilde{\beta}_{ij} \dot{\hat{\beta}}_{ij}$$

$$= r^T (M \ddot{q}_r + C \dot{q}_r + D - \tau - Cr)$$
$$+ \frac{1}{2} r^T \dot{M} r + \sum_{i=1}^{n} \sum_{j=1}^{l} \frac{1}{\gamma_{ij}} \tilde{\beta}_{ij} \dot{\hat{\beta}}_{ij}$$

$$= r^T (M \ddot{q}_r + C \dot{q}_r$$
$$+ D - Kr - \sum_{i=1}^{n} h_i \hat{\beta}_i - \mathbf{E}_{\max} \cdot sign(r) - Cr)$$
$$+ \frac{1}{2} r^T \dot{M} r + \sum_{i=1}^{n} \sum_{j=1}^{l} \frac{1}{\gamma_{ij}} \tilde{\beta}_{ij} \dot{\hat{\beta}}_{ij}$$

$$= r^T \left(\sum_{i=1}^{n} h_i \beta_i \right.$$
$$\left. - \sum_{i=1}^{n} h_i \hat{\beta}_i - Kr - \mathbf{E}_{\max} \cdot sign(r) - Cr \right)$$
$$+ \frac{1}{2} r^T \dot{M} r + \sum_{i=1}^{n} \sum_{j=1}^{l} \frac{1}{\gamma_{ij}} \tilde{\beta}_{ij} \dot{\hat{\beta}}_{ij}$$

$$= r^T \left(\sum_{i=1}^{n} h_i \beta_i^* \right.$$
$$\left. - \sum_{i=1}^{n} h_i \hat{\beta}_i - Kr - \mathbf{E}_{\max} \cdot sign(r) \right) + r^T \sum_{i=1}^{n} E_i$$
$$- \frac{1}{2} r^T (2C - \dot{M}) r + \sum_{i=1}^{n} \sum_{j=1}^{l} \frac{1}{\gamma_{ij}} \tilde{\beta}_{ij} \dot{\hat{\beta}}_{ij}$$

$$= - \sum_{i=1}^{n} h_i \tilde{\beta}_i r_i - r^T K r - \mathbf{E}_{\max} \cdot r^T sign(r)$$
$$+ r^T \sum_{i=1}^{n} E_i + \sum_{i=1}^{n} \sum_{j=1}^{l} \frac{1}{\gamma_{ij}} \tilde{\beta}_{ij} \dot{\hat{\beta}}_{ij} \tag{33}$$

Combining Eqs. (26) and (33), the relationship of Eq. (34) can be obtained as follows:

$$\dot{\boldsymbol{Q}} = -\boldsymbol{r}^T\boldsymbol{K}\boldsymbol{r} - \mathbf{E}_{\max}\boldsymbol{r}^T sign(\boldsymbol{r}) + \boldsymbol{r}^T\sum_{i=1}^{n}E_i$$

$$= -\boldsymbol{r}^T\boldsymbol{K}\boldsymbol{r} - \boldsymbol{r}^T(\mathbf{E}_{\max}\cdot sign(\boldsymbol{r})$$

$$-\sum_{i=1}^{n}E_i) \leq -\boldsymbol{r}^T\boldsymbol{K}\boldsymbol{r} - \sum_{i=1}^{n}(E_{i\_\max}-E_i)\,|r_i| \leq 0$$

$$(34)$$

Therefore, the stability condition is sufficient according to Eq. (34), which proves the stability of the proposed control law.

6 Numerical simulation

In this section, the validity of the proposed control strategy is verified with a planar dynamic model of a space robot with a 4-DOF robotic arm operating in the free-floating mode as established by the Matlab/Simulink software, as shown in Fig. 5. The sampling period is 0.001 s for the established simulation platform. The entire system operating in the post-capture stage has initial linear/angular motion with the initial angular velocity of 0.25 rad/s for a captured object during the pre-captured stage, in addition to precise knowledge about the spacecraft as well as the robotic arm and unknown dynamic parameters about the captured object in the end-effector. The geometric and inertial parameters of the system employed in the model are shown in Table 1, where a_i and b_i denote the position vector from the joint i to the centroid of link i and also from the center of link i to the joint $(i+1)$, respectively; I_i denotes the inertial tensor along the z axis; link 0 represents the spacecraft, and the attitude angle and joint angle can be expressed by α and θ_i, respectively. The parameter setting and initial condition of the model are illustrated by Table 2, and the interior disturbance term $\boldsymbol{d}$ in the robotic system is set by the function $d_i = (0.8 * \text{sign}(\dot{q}_i) + 5 * \sin(10t) + 2 * \boldsymbol{rand}(0,1))$ for each joint, where the signal of $\boldsymbol{rand}(0,1)$ means the value is randomly produced from the range of (0,1).

The total linear/angular momentum of the system in the post-capture stage is shown in Fig. 6, where the entire system is shown to be subject to the law of linear/angular momentum conservation. In the simulation, the adaptive reactionless path planning is considered via the SW-RLS algorithm and the conventional RLS algorithm, and the planned path via the two various algorithms can be obtained with the parameter set-
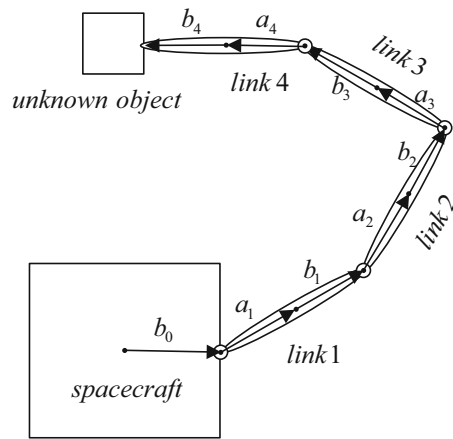

Fig. 5 Space robot with a 4-DOF robotic arm

Table 1 Geometric and inertial parameters of the space robot

Link i	Mass (kg)	a_i (m)	b_i (m)	I_i (kg· m^2)
0	500	–	0.4	500
1	10	0.25	0.25	0.5
2	10	0.25	0.25	0.5
3	10	0.25	0.25	0.5
4	10	0.25	0.25	0.5
Captured object	20	0.5	–	5

Table 2 Parameter setting of the dynamic simulation

Parameter	Value	Parameter	Value
$\boldsymbol{K}$	Diag (500, 500, 500)	$\alpha(0)$	0 (rad)
$\boldsymbol{\Lambda}$	Diag (2, 2, 2)	$\dot{\alpha}(0)/\omega_0$	0.1 (rad/s)
$c_1 = c_2$	0.2	$\theta_1(0)$	0 (rad)
w	2	$\theta_2(0)$	$\pi/2$ (rad)
$S_{\max} = -S_{\min}$	1	$\theta_3(0)$	0 (rad)
$V_{\max} = -V_{\min}$	1	$\theta_4(0)$	$-\pi/2$ (rad)
γ	1	$\dot{\theta}_i(0), i = 1, 2, 3, 4$	0 (rad/s)
m	20	$\boldsymbol{v}_0$	$[0.5\ \ 0.2]^T$
l	60		
$\dot{\boldsymbol{\xi}}$	$[1\ 1\ 1\ 1]^T$		
δ	1.2		
ε_i	2		

tings in Table 2 and illustrated in Fig. 7. It can be concluded that the planned path for the robotic arm via the SW-RLS algorithm exhibits a time-variable feature that
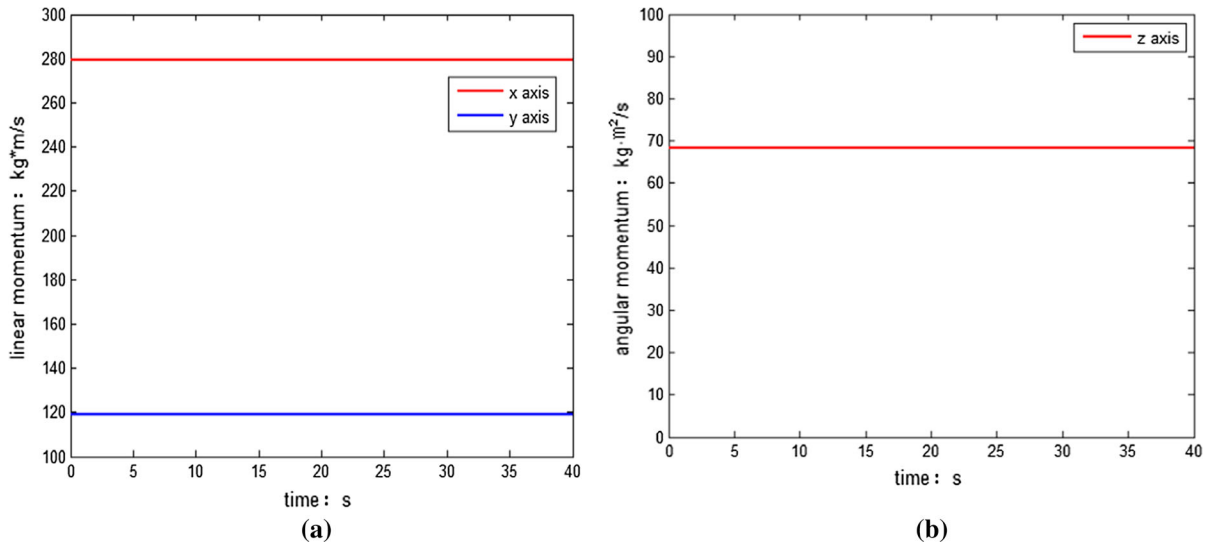
Fig. 6 Total linear/angular momentum measurement via Eq. (10)
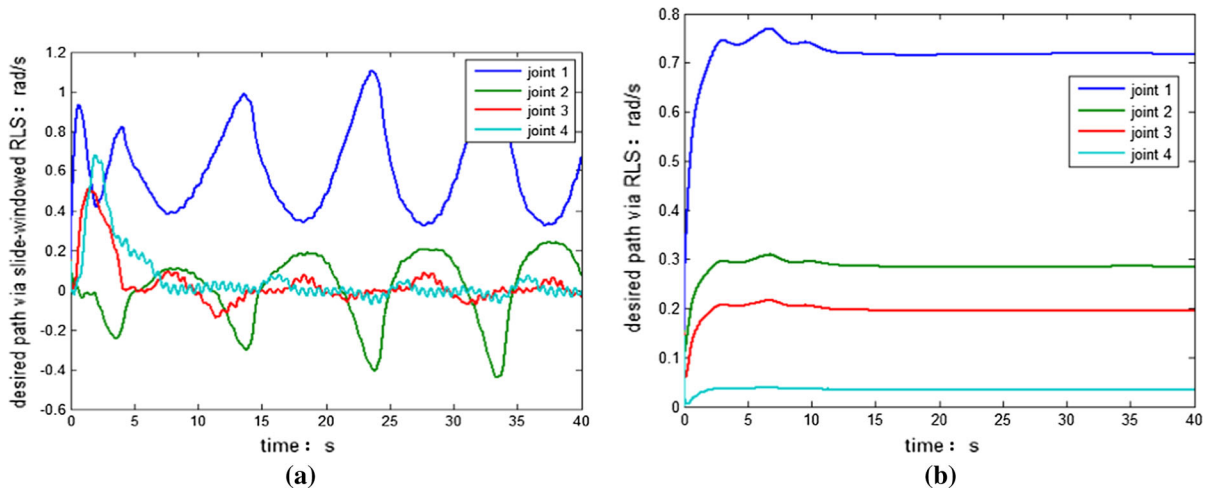

Fig. 7 Adaptive reactionless path planning via various algorithms

keeps pace with Eq. (16), yet the planned path via the conventional RLS exhibits a saturation phenomenon that cannot track the time-variable property of the coefficient matrix.

Then, several various control schemes are employed to track the planned path produced by the SW-RLS algorithm, expressed as follows:

Scheme 1. Adaptive control strategy via the RBF algorithm: 60 hidden layer nodes (l= 60); the adaptive law conforming to Eq. (26); the center f_{iC}, the width σ and the bias of hidden nodes affiliated with **rand**($-$1,1),

rand(0,1) and **rand**(0,1), respectively; the activation function selected by the radial basis function with $h_i = \exp(-(f_i(x) - f_{iC})^2/(2\sigma)^2)$; the output of controller $\hat{\tau}_i = \hat{\tau}_{PDi} + \hat{\tau}_{Ai}$ with corresponding K in Table 2.

Scheme 2. Adaptive control strategy via the ELM algorithm: all initial conditions are in accordance with scheme 1 except that the activation function is selected by the sigmoid function with $h_i = 1/(1 + \exp(-f_i(x)))$.

Scheme 3. Robust adaptive control strategy via the ELM algorithm: all initial conditions are
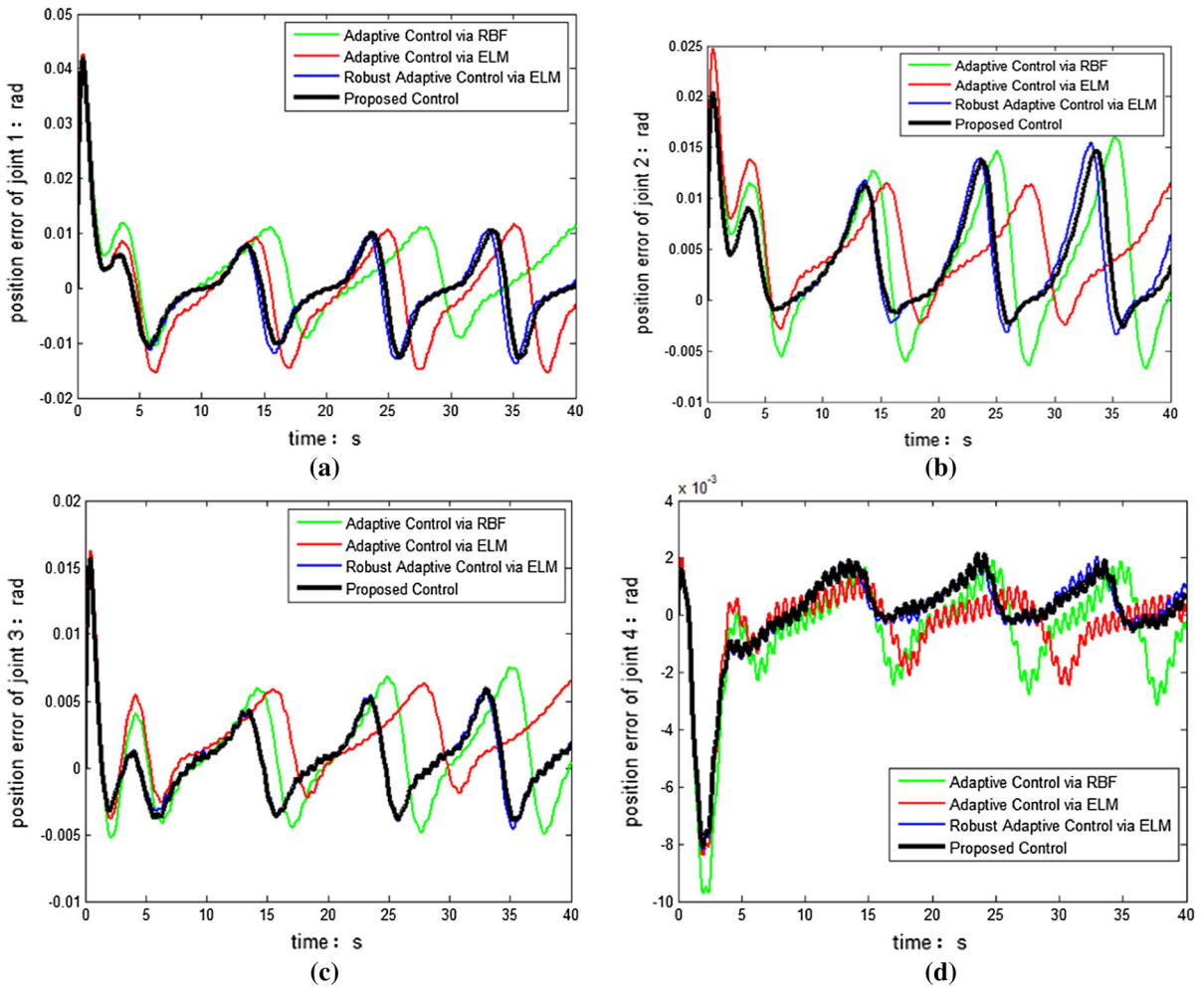
Fig. 8 Position tracking error of each joint controller via various control strategies

in accordance with scheme 2 except an appending robust controller with the output of $\hat{\tau}_i = \hat{\tau}_{PDi} + \hat{\tau}_{Ai} + \hat{\tau}_{Ri}$.

Scheme 4. Proposed control strategy: all initial conditions are in accordance with scheme 3 except the optimization of the input weight matrix for the ELM algorithm via the PSO.

The comparison of the tracking results for control Schemes 1–4 is shown in Fig. 8 and Tables 3, 4, with tracking performance and tracking error, respectively. Then, the angular velocity of the spacecraft is measured, as shown in Fig. 9, which exhibits the existing disturbance from the motion of the robotic arm to the spacecraft as well as to the attitude stability.

According to the tracking results from Fig. 8 and Table 3, the adaptive control strategy via ELM exhibits better speed performance compared with adaptive control strategy via RBF, although the accuracy performances of the steady-state error for the two schemes are both inferior to the robust adaptive control strategy via ELM because of the appending of the robust control strategy. The proposed control strategy via the PSO-ELM algorithm exhibits slight tracking accuracy improvement and shorter transient time; however, an extremely negligible delay of speed exists compared with the robust adaptive control strategy via the ELM algorithm, which reflects the optimization process of the PSO algorithm to seek and update the optimal input weight matrix of the network. In addition, Fig. 9 and Tables 5 and 6 exhibit the stability of the spacecraft atti-

Table 3 Mean values of position tracking errors for each joint controller (5–40 s)

Error (°)	Adaptive control via RBF	Adaptive control via ELM	Robust adaptive control via ELM	Proposed control
Joint 1	0.268	− 0.195	0.121	0.117
Joint 2	0.432	0.386	0.258	0.252
Joint 3	0.124	0.175	0.117	0.112
Joint 4	− 0.091	− 0.781	0.069	0.059

Table 4 Position tracking steady-state mean square errors for each joint controller (5–40 s)

Error (°)	Adaptive control via RBF	Adaptive control via ELM	Robust adaptive control via ELM	Proposed control
Joint 1	0.371	0.429	0.381	0.374
Joint 2	0.418	0.301	0.309	0.307
Joint 3	0.241	0.215	0.161	0.151
Joint 4	0.201	0.187	0.182	0.181

Fig. 9 Angular velocity measurement of the spacecraft via various control strategies
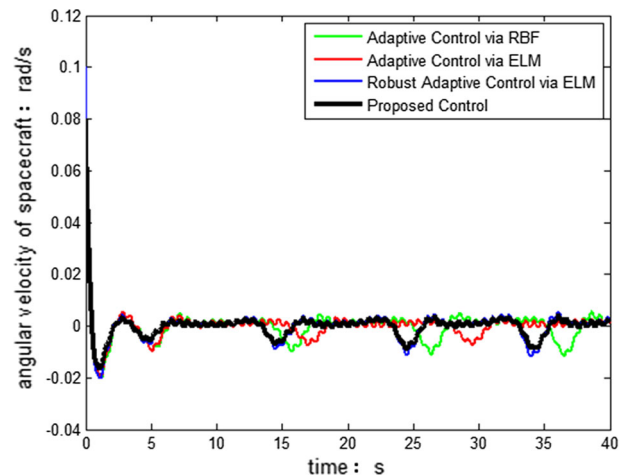
Table 5 Mean value of spacecraft angular velocity (5–40 s)

Error (°)	Adaptive control via RBF	Adaptive control via ELM	Robust adaptive control via ELM	Proposed control
	− 0.217	− 0.191	− 0.187	− 0.172

Table 6 Position tracking steady-state mean square of spacecraft angular velocity (5–40 s)

Error (°)	Adaptive control via RBF	Adaptive control via ELM	Robust adaptive control via ELM	Proposed control
	0.402	0.381	0.392	0.378

tude after capturing an unknown object, where the reactionless control strategy via the proposed scheme shows faster and relatively less angular spacecraft velocity as well as the least disturbance, which validates the proposed method in this paper.

7 Conclusion

An adaptive reactionless path planning and control integrated strategy is proposed for free-floating space robots while capturing unknown objects, achieving the reactionless motion of a robotic arm and ensuring the stability of the base attitude of the spacecraft. A SW-RLS algorithm is introduced to avoid the saturation feature and to construct adaptive reactionless path planning, and a composite control strategy via the PSO-ELM algorithm is proposed to track the dynamic changing planning path with the speed and accuracy enhancement of tracking performance. The notable feature of the proposed design is that it requires neither accurate system modeling nor any information about the unknown properties. Most importantly, the design can dynamically realize the reactionless path tracking performance although there are uncertain and abrupt dynamic parameters from the captured object. The simulation results validate the proposed method in this paper, which makes it significant for on-orbit operations in the future.

References

1. Flores-Abad, A., Ma, O., Pham, K., Ulrich, S.: A review of space robotics technologies for on-orbit servicing. Prog. Aerosp. Sci. **68**, 1–26 (2014)
2. Dubowsky, S., Papadopoulos, E.: The kinematics, dynamics, and control of free-flying and free-floating space robotic systems. IEEE Trans. Robot. Autom. **9**(5), 531–543 (1993)
3. Thai Chau, N.H., Inna, S.: Adaptive reactionless motion and parameter identification in post-capture of space debris. J. Guid. Control Dyn. **36**(2), 404–414 (2013)
4. Nenchev, D.N., Yoshida, K., Vichitkulsawat, P., Uchiyama, M.: Reaction null-space control of flexible structure mounted manipulator systems. IEEE Trans. Robot. Autom. **15**(6), 1011–1023 (1999)
5. Yoshida, K.: Engineering test satellite VII flight experiments for space robot dynamics and control: theories on laboratory test beds ten years ago, now in orbit. Exp. Robot. VII **22**(5), 209–218 (2000)
6. Piersigilli, P., Sharf, I., Misra, A.K.: Reactionless capture of a satellite by a two degree-of-freedom manipulator. Acta Astronaut. **66**, 183–192 (2010)
7. Fukazu, Y., Hara, N., Kanamiya, Y., Sato, D.: Reactionless resolved acceleration control with vibration suppression capability for JEMRMS/SFA, In: IEEE Interantional conference on robotics and biomimetics, pp. 1359–1364. Piscataway, NJ, USA (2008)
8. Murotsu, Y., Senda, K., Ozaki, M.: Parameter identification of unknown object handled by free-flying space robot. J. Guid. Control Dyn. **17**(3), 488–494 (1994)
9. Ma, O., Dang, H.: On-orbit identification of inertia properties of spacecraft using a robotic arm. J. Guid. Control Dyn. **31**(6), 1761–1771 (2008)
10. Aghili, F., Parsa, K.: Motion and parameter estimation of space objects using laser-vision data. J. Guid. Control Dyn. **32**(2), 537–549 (2009)
11. Chu, Z.Y., Ma, Y., Hou, Y.Y., Wang, F.W.: Inertial parameter identification using contact force information for an unknown object captured by a space manipulator. Acta Astronaut. **131**, 69–82 (2017)
12. Goodwin, G.C., Elliott, H., Teoh, E.K.: Deterministic convergence of a self-tuning regulator with covariance resetting. IEEE Proc. D Control Theory Appl. **130**(1), 6–8 (1983)
13. Guo, L., Ljung, L., Priouret, P.: Performance analysis of the forgetting factor RLS algorithm. Int. J. Adapt. Control Signal Process. **7**(6), 525–537 (1993)
14. Liu, H.Y., He, Z.Y.: Sliding-exponential window RLS adaptive filtering algorithm: properties and applications. Signal Process. **45**, 357–368 (1995)
15. Huang P. F., Yuan J. P., Liang B.: Adaptive sliding-mode control of space robot during manipulating unknown objects. In: IEEE international conference on control and automation, pp. 2907–2912. Guangzhou, Guangdong, China (2007)
16. Zadeh, S.M.H., Khorashadizadeh, S., Fateh, M.M., Hadadzarif, M.: Optimal sliding mode control of a robot manipulator under uncertainty using PSO. Nonlinear Dyn. **84**(4), 2227–2239 (2016)
17. Chu, Z.Y., Li, J.C., Lu, S.: The composite hierarchical control of multi-link multi-DOF space manipulator based on UDE and improved sliding mode control. Proc. IMechE Part G J. Aerosp. Eng. **229**(14), 2634–2645 (2015)
18. Faieghi, M.R., Delavari, H., Baleanu, D.: A novel adaptive controller for two-degree of freedom polar robot with unknown perturbations. Commun. Nonlinear Sci. Numer. Simul. **17**, 1024–1030 (2012)
19. Zhang, W.H., Ye, X.P., Jiang, L.H., Zhu, Y.F., Ji, X.M., Hu, X.P.: Output feedback control for free-floating space robotic manipulators base on adaptive fuzzy neural network. Aerosp. Sci. Technol. **29**, 135–143 (2013)
20. Smith, A.M., Yang, C.G., Ma, H.B., Culverhouse, P., Cangelosi, A., Burdet, E.: Novel Hybrid Adaptive Controller for Manipulation in Complex Perturbation Environments. PLoS ONE **10**(6), 1–19 (2015)
21. Chu, Z.Y., Cui, J., Sun, F.C.: Fuzzy adaptive disturbance-observer based robust tracking control of electrically driven free-floating space manipulator. IEEE Syst. J. **8**(2), 343–352 (2014)
22. Qin, L., Liu, F.C., Liang, L.H., Gao, J.F.: Fuzzy adaptive robust control for space robot considering the effect of the gravity. Chin. J. Aeronaut. **6**(27), 1562–1570 (2014)
23. Zhang, W.H., Qi, N.M., Ma, J., Xiao, A.Y.: Neural integrated control for a free-floating space robot with suddenly changing parameters. Sci. China **54**(10), 2091–2099 (2011)
24. Chen Z. Y., Chen L.: Robust adaptive composite control of space-based robot system with uncertain parameters and external disturbances. In: The 2009 IEEE/RSJ international conference on intelligent robots and systems, pp. 2353–2358, Louis, USA (2009)

25. Widrow, B., Lehr, M.A.: 30 years of adaptive neural networks perception, madaline, and back propagation. Proc. IEEE **78**(9), 1415–1442 (1990)

26. Huang G. B., Zhu Q. Y., Siew C. K.: Extreme learning machine: a new learning scheme of feedforward neural networks, In: Proceedings of international joint conference on neural networks, pp. 985–990. Budapest, Hungary (2004)

27. Rong, H.J., Wei, J.T., Bai, J.M., Zhao, G.S., Liang, Y.Q.: Adaptive neural control for a class of MIMO nonlinear systems with extreme learning machine. Neurocomputing **149**, 405–414 (2015)

28. Petković, D., Danesh, A.S., Dadkhah, M., Misaghian, N., Shamshirband, S., Zalnezhad, E., Pavlović, N.: Adaptive control algorithm of flexible robotic gripper by extreme learning machine. Robot. Comput. Integr. Manuf. **37**, 170–178 (2016)

29. Zhu, Q.Y., Qin, A., Suganthan, P., Huang, G.B.: Evolutionary extreme learning machine. Pattern Recognit. **38**(10), 1759–1763 (2005)

30. Kennedy, J., Eberhart, R.: Particle swarm optimization. In: Proceedings of the IEEE international conference on neural networks, vol. 4, pp. 1942–1948 (1995)

31. Xu, Y., Shu, Y.: Evolutionary extreme learning machine—based on particle swarm optimization. Lect. Notes Comput. Sci. **3971**, 644–652 (2006)

32. Han, F., Yao, H., Ling, Q.: An improved extreme learning machine based on particle swarm optimization. Lect. Notes Comput. Sci. **6840**, 699–704 (2011)

33. Figueiredo, E.M.N., Ludermir, T.B.: Investigating the use of alternative topologies on performance of the PSO-ELM. Neurocomputing **127**, 4–12 (2014)